The reliability of inverse modelling for the wide scale characterisation of the thermal properties of buildings

Alfonso P. Ramallo-González[1,4,*], Matthew Brown[2], Elizabeth Gabe-Thomas[3], Tom Lovett[2], David A. Coley[1].

[1]Department of Architecture and Civil Engineering, University of Bath.

[2]Department of Psychology, University of Bath.

[3]Department of Computer Science, University of Bath.

[4]Faculty of Computer Science, University of Murcia.

[*]Corresponding author.

Abstract

The reduction of energy use in buildings is a major component of greenhouse gas mitigation policy and requires knowledge of the fabric and the occupant behaviour. Hence there has been a longstanding desire to use automatic means to discover these. Smart meters and the internet-of-things have the potential to do this. This paper describes a study where the ability of inverse modelling to identify building parameters is evaluated for 6 monitored real and 1000 simulated buildings. It was found that low-order models provide good estimates of heat transfer coefficients and internal temperatures if heating, electricity use and CO2 concentration are measured during the winter period. This implies that the method could be used with a small number of cheap sensors and enable the accurate assessment of buildings' thermal properties, and therefore the impact of any suggested retrofit. This has the potential to be transformative for the energy efficiency industry..

Keywords: Energy efficiency; Inverse modelling; Lumped parameter model, Smart meter.

1. Introduction

Buildings are responsible for close to 40% of greenhouse gas emissions in developed countries , and there is a scientific consensus that these have triggered a change in the climate . However, it is known that a substantial reduction in energy use is possible from the built environment , making the built environment a major target for reduction policies.

Two key questions to reducing the energy demand of a building are: (i) how might the building be better used in order to minimise energy consumption? And, (ii) how effective might physical upgrades be? It is well known that relying on generic values for the impact of such changes: for example, that an x% change in U-Value, leads to a y% change in annual energy demand within the domestic housing stock, are inaccurate as they are based on generic assumptions, and show errors often larger than 70% . For an accurate estimate of either behaviour or fabric-related changes, an accurate thermal characterisation of the building and its use is therefore required.

The work presented in this paper is an attempt to understand and quantify the potential of deriving the thermodynamic properties of a building using Inverse Modelling (IM). In theory this should be possible if the precise state of the building and its environment is known at any time. This state would include all room temperatures, the solar, heating, metabolic and other gains, and the weather. Even within the setting of a research project such monitoring would be difficult to achieve, and clearly impossible as a general technique. In this study, IM was tested when the state is not completely known due to technical limitations - as would be the case if the approach were used as part of an advanced smart meter rollout across many buildings. To do this, six buildings were fitted with simple sensors of the form that might be representative of an advanced smart meter and monitored in winter. And in addition, computer models of 1000 further buildings were used to examine the best form of inverse model and smart meter sensor set, and ensure the results could be generalised to buildings of

a wide variety of constructions and occupant behaviours and different seasons. This should be contrasted with previous work on the topic where buildings have been instrumented in a research setting with a large number of highly accurate sensors .

2. Background

The term Inverse Modelling is used to describing a modelling technique that uses the inputs and outputs of a system to obtain a mathematical description of it. This technique can be contrasted with direct modelling, in which a mathematical representation of the system is created from known physical principles (equations) and system characteristics. In general, inverse modelling aims to look for the simplest model capable of capturing the recorded behaviour of the system.

The generic method used in inverse modelling is shown below :

1 – Record inputs $u(t)$ and outputs $y(t)$ of the real system.
2 – Use the inputs $u(t)$ within a model with parameters (θ) to generate the prediction $\hat{y}(t,\theta)$.
3 – Compute the error $\varepsilon(t,\theta) = \hat{y}(t,\theta) - y(t)$
4 – Determine the parameter vector $\hat{\theta}$ that minimises a norm (ρ) of the predicted error:

$$\hat{\theta} = \underset{\theta}{\operatorname{argmin}} \sum_{t} \rho(\varepsilon(t,\theta))$$

In the work presented in this paper, the inputs to the system are the measured energy use and other gains and losses, and the output the internal temperature of the building; and both, inputs and outputs vary with time. The two are linked by the model, i.e., the building. Embedded in this model are elements such as U-values or ventilation.

IM has been used to address a variety of problems in building science, including: Ghiaus' work on temperatures within buildings ; Rabl and Rialhe's work on energy signature models in commercial buildings ; the work of Wang and Xu that used a genetic algorithm to estimate the parameters of a model representing a commercial building ; Bacher's and Madsen's study

that evaluated model topologies ; Lundin et al. development of a method to estimate global parameters (total heat loss, total heat capacity and total gain factor); of test cells using neural networks , and the work of Yang et al. who used dynamic artificial neural networks that are able to capture variations in the behaviour of the model . More recently Date et al. have compared the performance of simple and complex LPMs for modelling the thermodynamics of test houses .

IM has also been applied in Model Predictive Control (MPC). This technique uses an online generated building dynamic model to control the building services and optimise energy use. One of the first examples of this was the work of Coley and Penman , and more recently the work of Kolokotsa et al. . Also Cole et al. used simple models combined with EnergyPlus to implement MPC and Široký et al. performed predictive control of the heating system together with weather predictions in .

In this work, the reduced building model is a Lumped Parameter Model (LPM). Such models had been used in previous inverse modelling studies of buildings . Examples of various LPMs can be found in Appendix II.

3. Method

The work presented here is focused on discovering if IM can be used across a large variety of domestic buildings and using a minimum number of sensors. A large number of buildings (approx. 1000) with a variety of possible sensors was needed. This is only realistic if most of the buildings were models, with a small group of real buildings being used for validation.

3.1. Creation of the models

The creation of the synthetic stock of 1000 building models proved to be non-trivial due to the importance of ensuring their fidelity to the real stock. Sixteen representative variables were used to characterise the geometry, building fabric and occupant habits; and each one of these was sampled from a different probability distribution from surveys of real buildings. The parameters can be seen in Table 1. The ranges and definitions of these parameters and the data sources used are described in Appendix I. Although unlikely, it is possible that the sampling of the probability distributions led to an unrealistically extreme value. To avoid this, fixed deterministic limits have been used to ensure valid simulation inputs. The limits are also shown in Table 1.

Table 1 – Variables used to generate each one of the building models in the synthetic building stock.

Variable	Distribution	Lower limit	Upper limit
1. House type	Discrete probability (see appendix)	n/a	n/a
2. Floor area	Lognormal, a= 4.46, b= 0.17	16	800
3. Number of floors	Discrete [1, 2, 3]	n/a	n/a
4. Shared walls	Discrete [1, 2]	n/a	n/a
5. Aspect ratio	Uniform	0.33	3
6. Wall U-Value	Lognormal, a = -0.43, b = 0.62	0.1	3.02
7. Roof U-Value	Lognormal, a = -0.13, b = 0.24	0.1	2.35
8. Infiltration	Lognormal, a= -0.978, b= 0.20	n/a	n/a
9. Fenestration	Normal, a=0.19, b=0.05	0.075	n/a
10. Window type	Discrete [Single, Double, Triple]	n/a	n/a
11. Thermal mass (mm)	Normal, a=50, b=20	5	n/a
12. Domestic hot water use [kWh/m2]	Normal, a=18, b=1.15	0	n/a
13. Occupants' activity [W]	Discrete [70, 80, 120]	n/a	n/a
14. Surrounding obstacles	Uniform	0	1
15. Electricity use [kWh/m2]	Normal, a = 38.1, b = 17.95	10	Inf.
16. Ventilation [m3/s]	Normal, a = 0.0035, b =0.001	0	Inf.

3.1.1. Generation of time series data from the synthetic building stock

Having created the building models, simulations of the buildings were carried out using EnergyPlus . The buildings were modelled as single-zones and as parallelepipeds with the

number of faces in contact with the outside dependent on the architype. The time discretisation for solving the model equations was five minutes and the reporting period one hour. The heating was set to maintain a temperature of 21 degree Celsius when occupied in winter and a setback temperature of 17 degree Celsius for the whole year. The heating system consisted of radiators with a nominal power limited in each case corresponding to that value likely to be found in the real building. The simulations were performed using the London weather file for EnergyPlus . Examples of the time series output can be seen in Figure 1 and Figure 2.

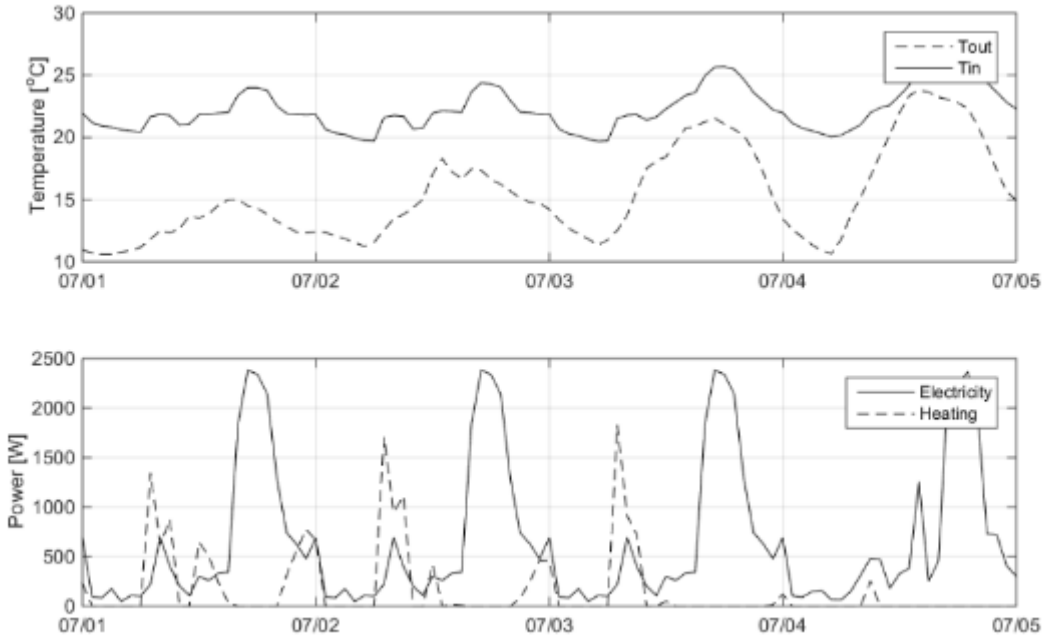

Figure 1 – Internal temperature, external temperature and electric gains during four days in June.

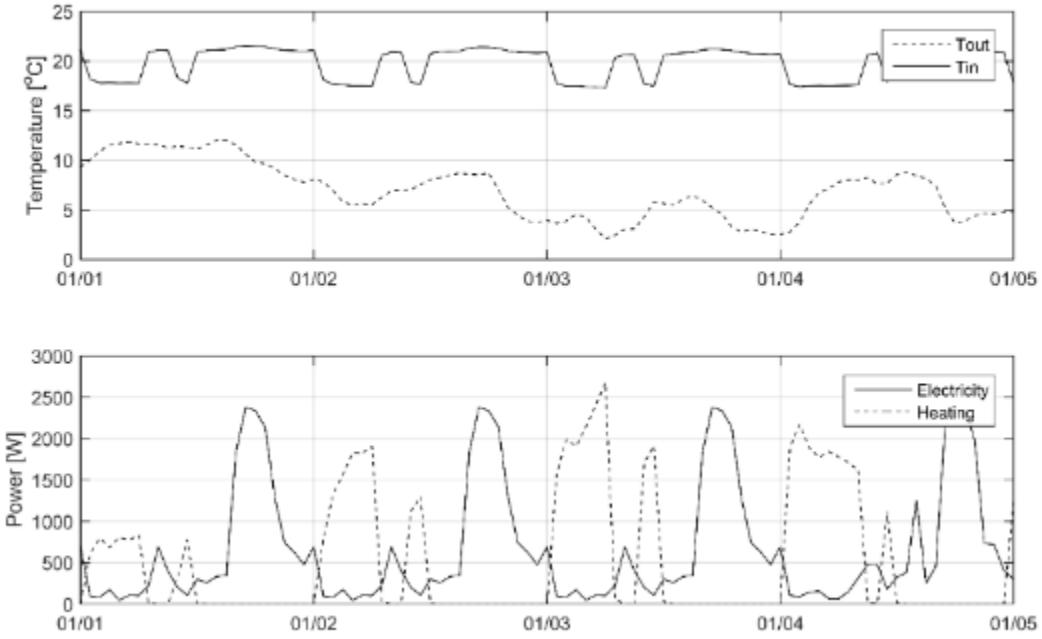

Figure 2 – Internal temperature, external temperature, electric gains and heating during four days in January.

3.1.2. Evaluation of the SBS

Once the synthetic building stock (SBS) was created, the Heat Transfer Coefficient (HTC) of each building was calculated.

The range of HTCs in the SBS and calculated with the distribution of heating from the Homes Energy Efficiency Database can be seen in the boxplot of Figure 3.

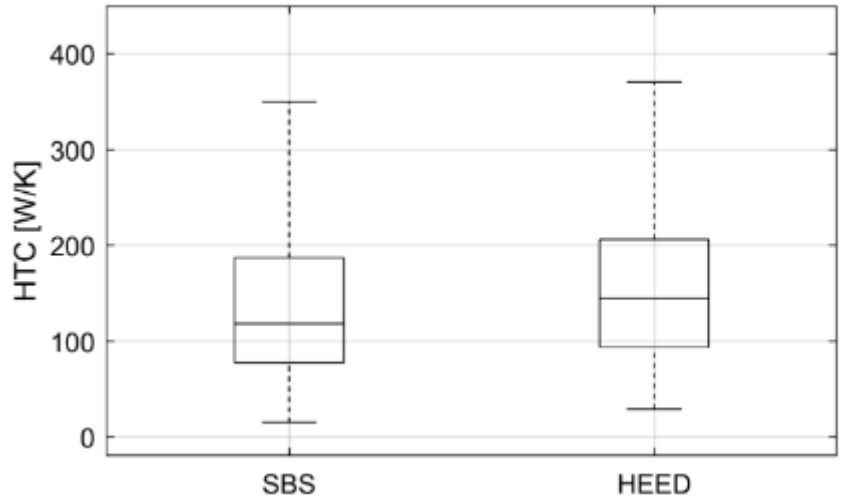

Figure 3 – Boxplots of the HTCs of the buildings of the synthetic building stock generated for this work and derived from the Home Energy Efficiency Database.

The thermal inertia of a building indicates the time that it takes to heat up or cool down. Heavy weight buildings have higher thermal inertia whereas light weight buildings have lower thermal inertia.

The LPM calculated with inverse modelling should also be capable of providing the thermal inertia of the building by giving the time constant of the model found by the IM engine. To calculate the real time constant of the building, the methodology given in BS EN ISO 13786:2007 was used. This method uses the effective thermal mass of the building together with the to gives the time constant .

The real time constants of the building in the synthetic building stock calculated with the BS EN ISO can be seen in Figure 4. According to the standard, it is normal to overestimate the thermal capacity of the building with this method of calculation, also the infiltration losses are not considered in the total heat transfer coefficient of the buildings for this work. These two factors make the time constant slightly bigger than in reality.

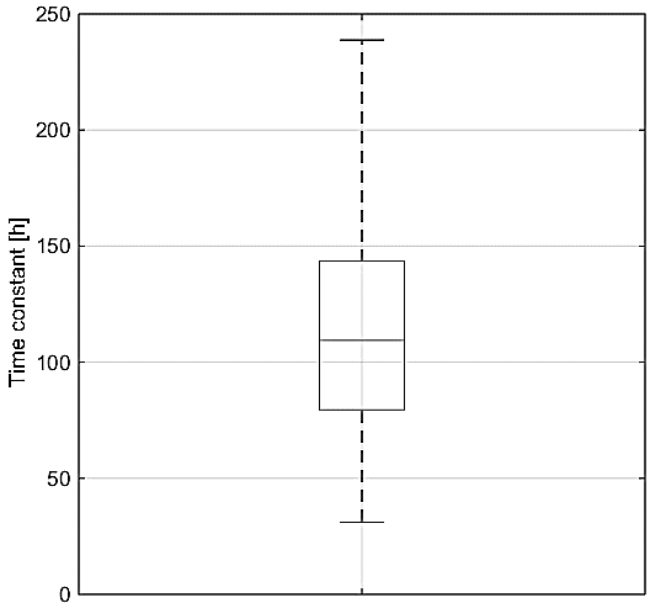

Figure 4 – Boxplot of the time constants of the buildings in the synthetic building stock. Clearly, a wide variety of buildings exist within the synthetic stock.

3.2. Choice of reduced model

Having created the stock of 1000 buildings, the next issue is the exact choice of the topology of the reduced model that will be used in the IM framework.

Most of the literature on inverse modelling is case specific, i.e. the researchers applied inverse modelling to one specific building and used a topology that was likely to work well for that building . In our case, a topology was needed that will work for most buildings and has the lowest complexity.

Eight possible model topologies were tested (see Appendix II for diagrams and explanation). The models are chosen for their previous use in the literature: Matthew et al. showed that a first order LPM (2R1C) can represent the thermo-dynamics of the building . Later, several authors such as Coley and Penman suggested a second order model with three resistors and two capacitors (3R2C), and stated that this model would fit buildings in an accurate way, but this was only tested with one building in each study . Another second order

model can be found in the works of Kampf et al. , in this case, the second order model has only two resistors and corresponds to the 2R2C of this paper. There are therefore first and second order LPMs in the literature that claim to represent building well. Tindale et al introduced however the internal thermal mass in the LPM this made the model third order. The thermal mass was included in a subset of LPMs used in this paper. This subset has the suffix TM, and increase by one the order of the LPM. For completeness we have added the one resistor and one capacitor LPM and a simple steady-state resistance (1R). Summarising we have used: 1R, 1R1C, 2R1C, 2R2C, 3R2C, 1R1CTM, 2R1CTM, 2R2CTM.

Ten random buildings within the SBS (see Appendix I) were tested using a two week period in March for all the model topologies. The goodness of the fit (i.e. the accuracy of predicting the correct internal temperature) was evaluated using the Adjusted R^2. The R^2 of the fitting represents the proportion of the variance of the original curve given by the estimated series, this means that a fitting with an R^2 of 1 represents a perfect fit. The Adjusted R^2 ($AdjR^2$) is a modification of the R^2 in which its value is penalised with the number of parameters in the model being fitted: the larger the number of parameters in the model, the smaller the $AdjR^2$. This is needed to perform a fair comparison of models with different numbers of adjustable parameters.

Figure 5 shows the $AdjR^2$ for the different models (the 1R model has been removed from the graph as it gives values of $AdjR^2$ smaller than 0).

Clearly, the 1R and 1R1C models perform poorly, and although higher orders imply a better fit, the gain is slight for any model more complex than the 2R1C model. It is also clear in this graph that the performance of the fit (as measured by $AdjR^2$) depends on the building.

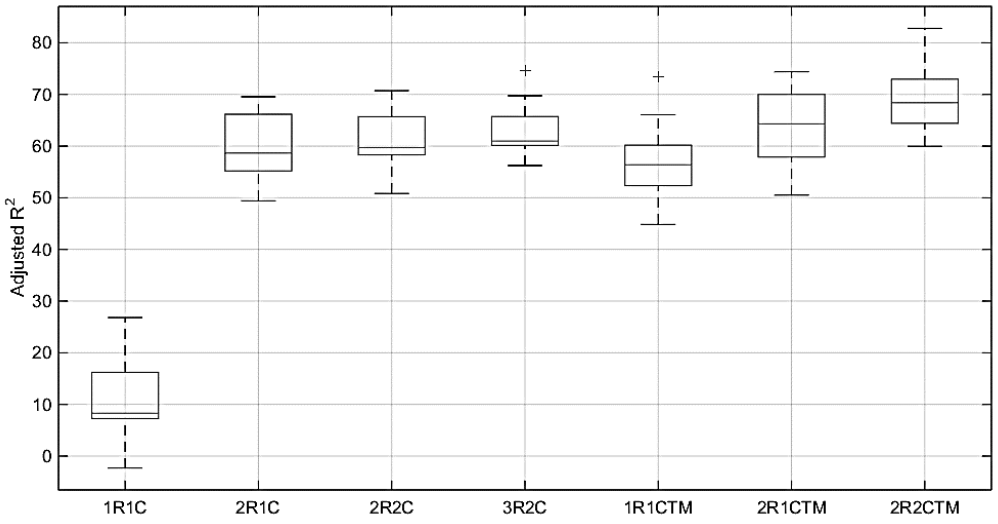

Figure 5 - Performance of the various models based on their ability to reproduce the temperature time series. Each boxplot includes ten building models (Results from 1R not included in the graph as they are negative).

The performance of the IM engine can also be measured by how close the estimated building parameters are to the parameters of the original EnergyPlus model. To calculate each one of the HTCs of each one of the EnergyPlus models, the areas of all surfaces were used together with their U-Values. This gave the UA for each one of the building elements. The summation of all the UAs gave the HTC of the model/building. Due to the way in which ventilation and infiltration is handled in this paper (considered independent heat losses) their effect is not included in the HTC calculation. Figure 6 shows the errors in estimations of the HTCs using inverse modelling in comparison with the HTC obtained from the EnergyPlus model for the eight different model topologies.

Figure 6 also shows that a quantitative leap in error occurs when going from the 1R1C model to the 2R1C model. It should be noted that there is an error even with the most complex models; this is due to the different methods of estimating the HTC—analytically and empirically.

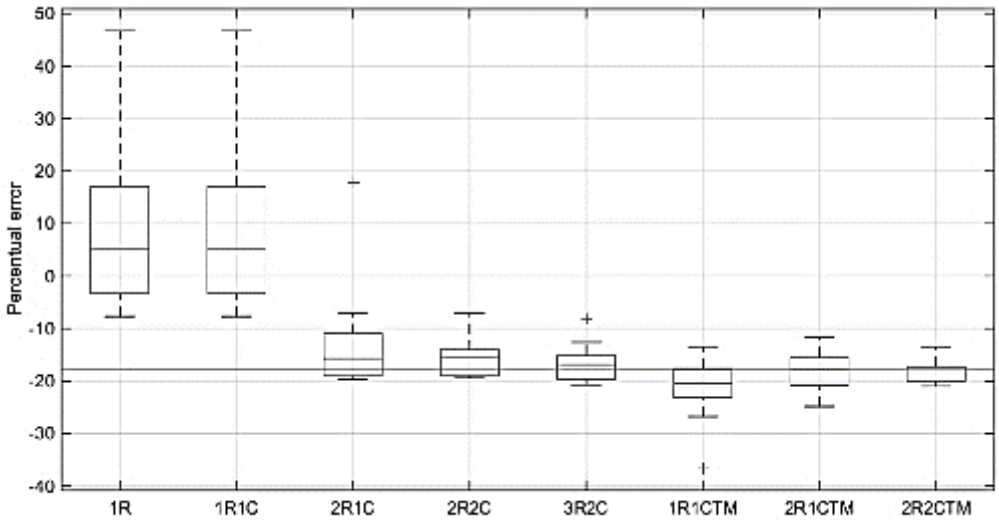

Figure 6 – Error in the calculation of the HTC using the fitted LPM with respect to that calculated from the EnergyPlus model, line at 17.1% corresponds to the median error for the 2R2CTM model used as a reference.

It should be noted that each extra parameter introduced into the LPM increases the decision space exponentially (leading to a substantial increase of the optimisation time) and can lead to identifiability problems (i.e. several set of parameters give the same response). Considering this, and seeing the performance of the 2R1C model topology, this model was chosen for the rest of the work.

3.3. Experimental Setup

The work presented in this paper aims to evaluate the applicability of inverse modelling to a stock of dwellings of very different sizes, construction standards and occupational patterns that have been all obtained from real surveys, but when the times series of gains etc. is only partially known due to a lack of sensors.

The gains and losses are applied directly to the interior of the building (the thermal zone) when using the LPM. The driving forces are therefore:

$$Q_{total} = Q_{solar} + Q_{electricity} + Q_{DHW} + Q_{matabolism} - Q_{infiltration} - Q_{ventilation} + Q_{heating}$$

Where Q_{solar} is the solar radiation that reaches the zone[1]. $Q_{electricity}$ is the total electrical power. Q_{DHW} is the heat from domestic hot water (DHW) that ends up in the zone. $Q_{metabolism}$ is the heat gain produced by the occupants. $Q_{infiltration}$ is the heat loss from hot air leaving the zone and being replaced by cold air via infiltration; $Q_{ventilation}$ is the equivalent from opening windows and $Q_{heating}$ is the heat delivered by the heating system.

Seven scenarios were created to represent the incompleteness of data that might be provided by an advanced smart meter or building management system. In each of these, one of the gains is unknown to allow pair wise comparison. For example, when the gain to the zone from domestic hot water (DHW) is deemed unknown, it is assumed that all the energy used to produce the DHW is all a heat gain within the building, whereas in truth most would simply flow down the drain (this is equivalent to only having a gross gas meter reading). Details about each scenario are given in Table 2.

Table 2 - Scenarios used.

Scenario number	**Missing information**	**Assumption in the IM engine**
0 (baseline)	None	All
1	Solar	Solar gains = 0
2	Electricity	Electricity use = 0
3	DHW	The heat used to heat up the DHW is considered to be all delivered to the thermal zone
4	Metabolism	Metabolic gains = 0
5	Infiltration	Heat loss due to infiltration = 0
6	Ventilation	Heat loss due to ventilation = 0
7	Heating	Heating = 0

As the model chosen has only three parameters the existence of local minima is unlikely, hence the optimisation method used was the Simplex method. Despite this, and to ensure the

[1] There is no rad-air node in this model topology to take radiative gains such as solar separately from convective gains, so they are all in the internal node.

identification of global minima, the optimisation was run 20 times for each building, each one with a different (random) starting point, and the best solution chosen as the global minima.

The model to be used was the 2R1C for the reasons explained in Section 3.2. The model has as inputs the outside temperature at the node representing the outside (n_0) and the gains at the node representing the interior of the building (n_i). The model can be seen in Figure 7.

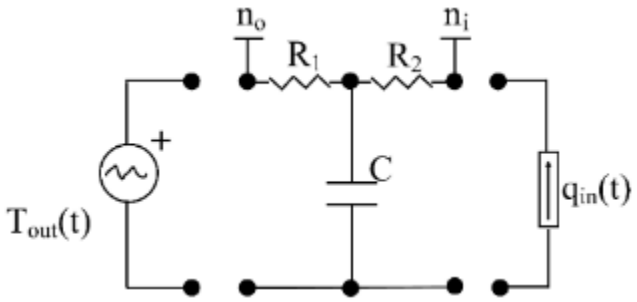

Figure 7 - Lumped parameter model 2R1C in the centre. The elements on the left and the right are the voltage source representing the outside temperature and the current source representing the gains respectively.

The inverse modelling was performed using three months of data from the EnergyPlus models: January, April and July. These three months were chosen as they are representative of winter, spring/autumn and summer.

Given seven scenarios, one thousand buildings, and three monthly periods the total number of model identifications was 24,000. The average time for each building estimation was around 20 seconds on a 4 core machine at 2.8GHz running single threaded.

Validation was then carried out for 6 buildings that were fitted with the type of sensors that might be at the core of an advanced smart metre rollout. In the set of real buildings, the air renewal is calculated via the concentration of CO_2, and only solar, DHW and metabolic gains are unknown.

4. Results and discussion

The final 2R1C LPM is that which gives the best fit with respect to internal temperature for a particular building and scenario, this is the one with the smallest sum of least squares of the errors. The two resistors of the LPM added together are equivalent to the total thermal resistance of the envelope; the inverse of this resistance is the Heat Transfer Coefficient (HTC) of the house. As the model used is a dynamic one, the time constant of the building envelope is also estimated - this is given by the product of the capacitance (C, representing the thermal mass) and the internal resistance of the model (R_2, Figure 7).

4.1. Baseline

The baseline (i.e. sensors measuring all gains and losses fitted to the 1000 houses) was the first scenario. This therefore established a bottom line for the precision of the method.

The HTC obtained by the IM algorithm was then termed the *estimated* HTC and the HTC of the EnergyPlus model termed the *real* HTC. The comparison of these two can be seen in Figure 8 as grey dots. There is a clear proportional offset, hence the estimations were adjusted to be centred over the y=x line, and the adjusted estimations are plotted as black dots.

Figure 8 shows that the error in estimation is proportional to the HTC, this means that the error in percentage terms of the HTC could be used to build the confidence intervals of the estimations. The value of the estimation error for the three months is shown in Table 3, Table 4 and Table 5. A 95% interval was used for the calculation of these errors. In the baseline the error for January is 8.5%. This implies that if all gains and losses are known and the inverse modelling engine was used to estimate the HTC of a dwelling (despite size, construction, fenestration ratio and so forth being unknown) the error in the estimation of the HTC of a

dwelling would have a 95% chance of being lower than a +/-8.5% range. This is an extremely good result given the variety of buildings represented.

The confidence intervals for the estimations were calculated once any solutions lying outside of the feasible space were eliminated and the estimations adjusted. The adjustment factors, confidence intervals and rate of convergence to a feasible solution are shown in Table 3, Table 4 and Table 5.

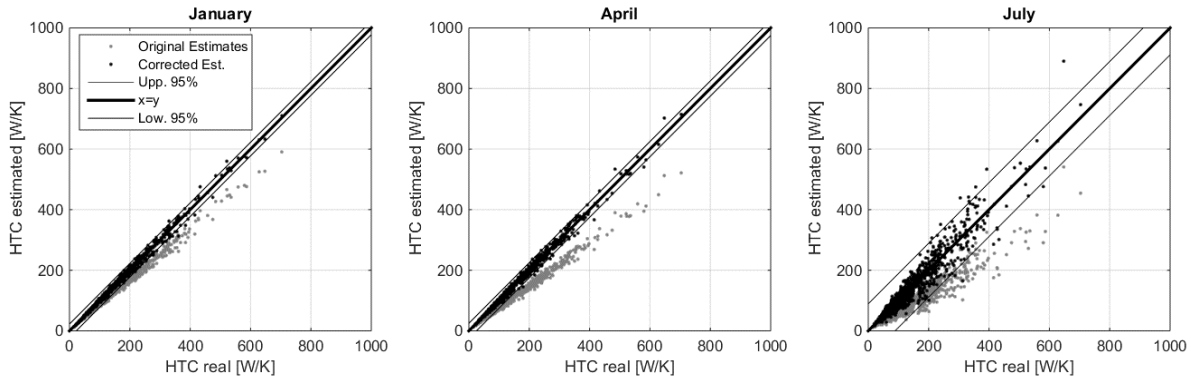

Figure 8 - Real and estimated HTC for the baseline. The grey dots are the original estimations, the black points represent the adjusted points. The lines of prediction at a 95% interval confidence are also shown.

It can be seen in these results that inverse modelling is accurate and robust with respect to the estimation of the total conductivity of the envelope and any errors small (especially when compared with reported errors in direct modelling of the order of the 200%). The error is maintained across all the buildings tested despite their large variability. This is already an important finding, as the LPM is much simpler than any direct model, and the assumed driving forces (such as weather) have been highly simplified.

Also, the ability of the inverse modelling engine to correctly obtain the time constant of the building was also studied. For this, the time constant of the estimated LPM was compared with the time constant obtained from the test described in Section 3.1.2 and considered as the

real time constant of the building. The time constant of the LPM was calculated as $\tau = R_1C$ (Figure 7). The estimated and real time constant for all buildings is compared in Figure 9.

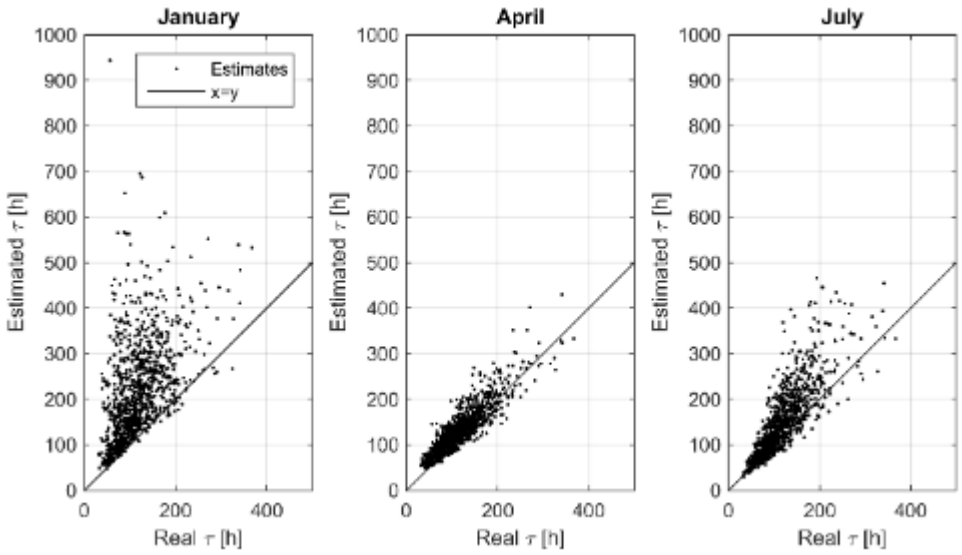

Figure 9 - Comparison between estimated and real time constant for each building.

The graphs show that in the case of the time constant of the building, the performance of the inverse modelling is best in April; this is expected, as the heating dominated regime in January makes it more difficult for the engine to capture the thermal inertia of the building. In August the time constant is still better estimated than in January, but worse than in April.

Another important metric is the goodness of the fit to the real internal temperature. If this is accurate, it would be possible to evaluate comfort parameters in the future or use model predictive control.

A graph of the time series is shown in Figure 10 as an example; the time series from the other 1000 EnergyPlus models are similar. This shows 7 days in January for House 1. It can be seen how fluctuations in the temperature are driven by the heating system as one may expect. The LPM is able to represent these temperature swings and the response time of the building. The $AdjR^2$ is 0.74.

Figure 11 shows the same house in summer. Again, the estimated internal temperature series follows the time series from EnergyPlus well. The Adjusted R^2 is 0.86.

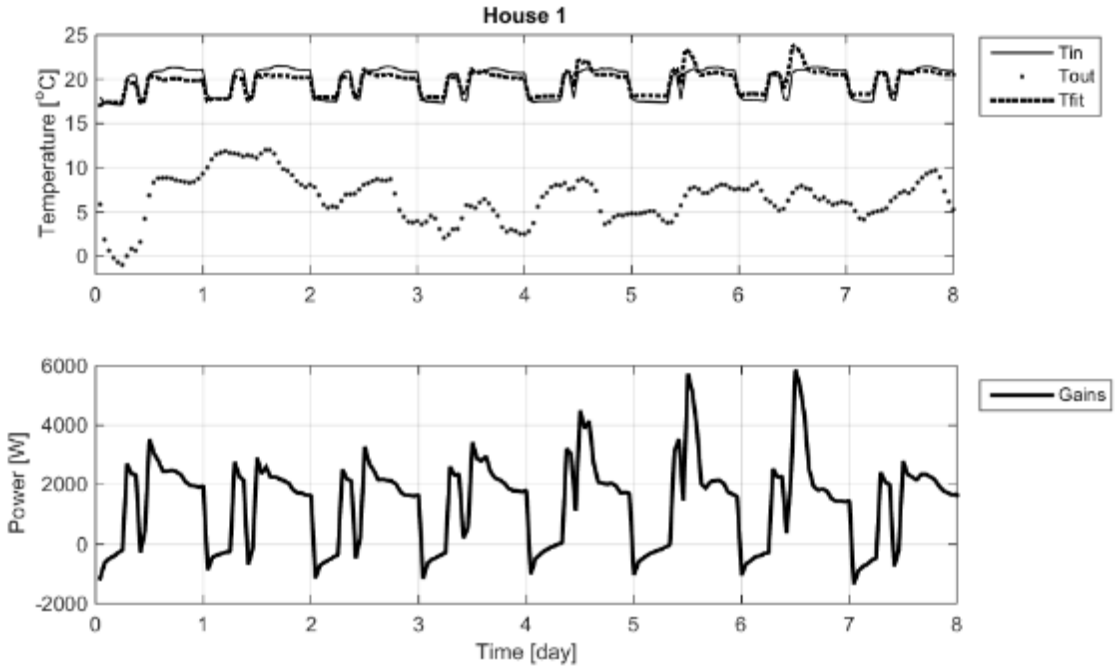

Figure 10 - Temperatures and gains for House 1 during 7 days in January. In the upper subplot the dashed line is the internal temperature generated by the adjusted LPM, the solid line is the internal temperature generated by EnergyPlus, the dotted line is the external temperature. The total net gains are represented in the bottom subplot. The fitting has an AdjR^2 of 0.74.

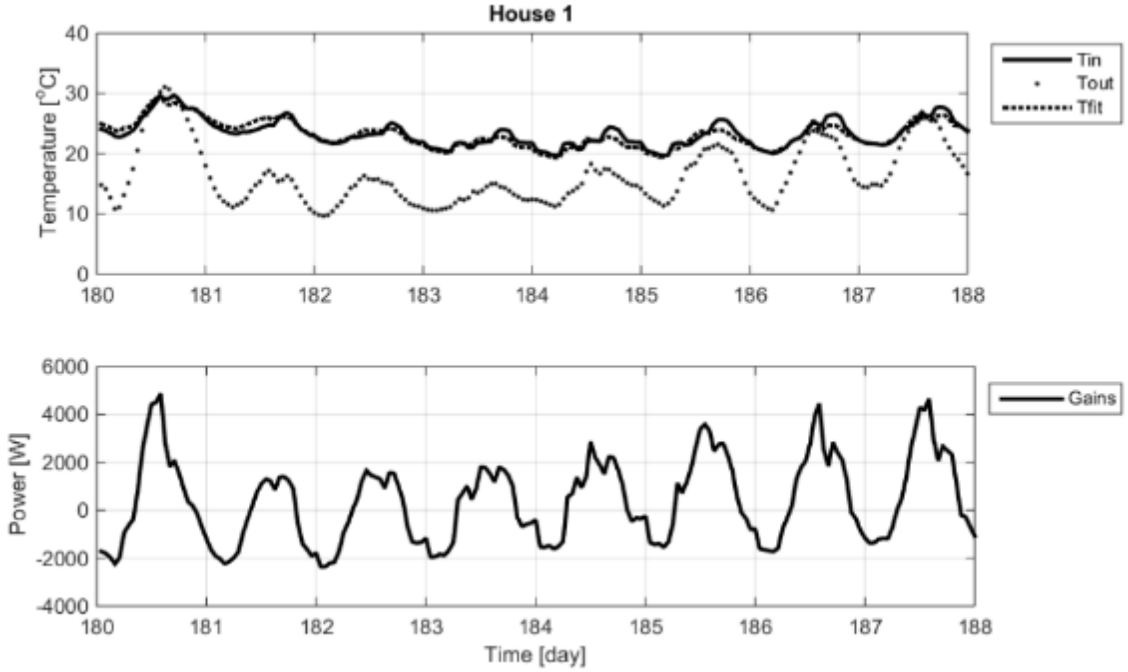

Figure 11 – Temperatures and gains for House 1 during 7 days of July. In the upper subplot the dashed line is the internal temperature generated by the adjusted LPM, the solid line is the internal temperature generated by EnergyPlus, the dotted line is the external temperature. The total net gains are shown in the bottom subplot. The fit has an AdjR^2 of 0.86.

4.2. Inverse Modelling with missing driving forces

Having shown the results of the IM framework with all the gains and losses known, the approach was applied to each scenario in turn, with each scenario representing the case when only some data could be gathered by the smart meter.

4.2.1. Estimation of Heat Transfer Coefficients

For the scenarios with missing knowledge of gains, correction factors corresponding to a linear adjustment of the type 'HTC_{real} = m x HTC_{est} + n' can be applied to improve the fit. It should be noted that the results from EnergyPlus should not be taken as ground truth; in some cases, researchers may want to give preference to the HTCs calculated with real data. However, the adjustment parameters for situations where some of the data are missing could

still be valid as they are the result of pair-wise comparison. This has application in real world problems (will be shown in section 4.3).

The factors can be seen in in Table 3, Table 4 and Table 5. These tables also show the number of infeasible solutions that were removed (those with negative resistance values in the LPM or negative $AdjR^2$). The tables also include the error in estimation. A maximum error in estimation of 20% means that if the IM engine gives an estimated HTC of 100 W/K the real HTC has a 95% probability of falling within the range 80-120 W/K. These maximum errors are also shown in Figure 12 for all scenarios and time periods.

Table 3 - Adjustment factors for the estimation of HTCs when one of the driving forces is missing, together with failure rate of the algorithm and the error in estimation. All for January.

Unknown gain	m [1]	n [W/K]	Fails [%]	Max. error in estimation [%] (+/-)
All gains known	1.210	-4.441	0.0	8.51
Electricity	1.331	5.131	0.8	38.36
DHW	0.903	-2.642	0.7	15.21
Infiltration	0.635	3.998	0.6	69.83
Metabolism	1.041	0.819	0.1	7.98
Solar	1.119	-2.116	13.7	17.96
Ventilation	0.971	-0.943	0.0	10.71
Heating	5.412	-37.561	61.9	161.95

Table 4 - Adjustment factors for the estimation of HTCs when one of the driving forces is missing, together with failure rate of the algorithm and the error in estimation. All for April.

Unknown gain	m [1]	n [W/K]	Fails [%]	Max. error in estimation [%] (+/-)
All gains known	1.377	-3.013	0.0	8.90
Electricity	1.564	3.520	3.6	52.80
DHW	0.877	-1.017	0.0	16.06
Infiltration	0.609	4.171	0.5	71.35
Metabolism	1.055	0.939	0.1	9.30
Solar	2.364	-9.793	9.9	72.47
Ventilation	0.968	-0.819	0.0	12.28
Heating	2.370	-32.337	14.1	105.75

Table 5 - Adjustment factors for the estimation of HTCs when one of the driving forces is missing, together with failure rate of the algorithm and the error in estimation. All for July.

Unknown gain	m [1]	n [W/K]	Fails [%]	Max. error in estimation [%] (+/-)
All gains known	1.653	-4.240	0.0	32.06
Electricity	2.234	-5.008	25.6	80.63
DHW	0.687	1.010	0.6	38.08
Infiltration	0.574	4.302	0.5	80.40
Metabolism	1.092	-0.563	0.1	36.34
Solar	6.290	-43.737	74.9	87.51
Ventilation	0.823	-6.194	0.0	77.80
Heating	1.046	-3.392	0.2	37.13

The results show that the inverse modelling engine can be highly reliable when all the gains are known (baseline), with a failure rate in winter of 0.0%.

It can be seen how the baseline adjustment parameter is larger than one. This means that the estimated HTC is smaller than the true HTC.

In scenarios *DHW*, *Infiltration* and *Ventilation*, the estimated HTC is greater than the true value. These represent the scenarios in which (1) all the power used to generate the DHW is mistakenly considered to be used for heating, (2) the infiltration is not considered and (3) the ventilation is ignored. Hence in these situations there is a heat loss that is not considered and therefore the inverse modelling engine captures that the gains required to maintain the internal temperature are smaller than they really are, resulting in an overestimation of the HTC.

The results show that the combined measurement of heating and DHW widens the confidence intervals of the estimations. An extra sensor in the DHW main pipe may be a cost effective measurement to reduce this source of error.

The results show that in April and July, the engine needs to have some estimate of the solar gains to make the algorithm converge for the majority of the dwellings. This would result in a substantial increase in the resources needed in terms of measuring equipment. The obvious solution to this challenge is to perform this type of experiment in the cooler months

when the contribution of solar energy to the gains of the building is small. If an accurate estimation of the model wants to be carried out in the summer months a more complex LPM needs to be used that can differentiate between radiative and convective gains, and a more detailed knowledge of the solar gains will be needed. The latter would be rather difficult to obtain cheaply for a large number of dwellings.

It can be seen from the tables that the results when heating is unknown in January and April are very poor, with large errors and much larger adjustment parameters. Not knowing infiltration and ventilation also introduces substantial errors. This suggests that sensors that give an indication of air renewal such as CO_2 sensors would be worthwhile.

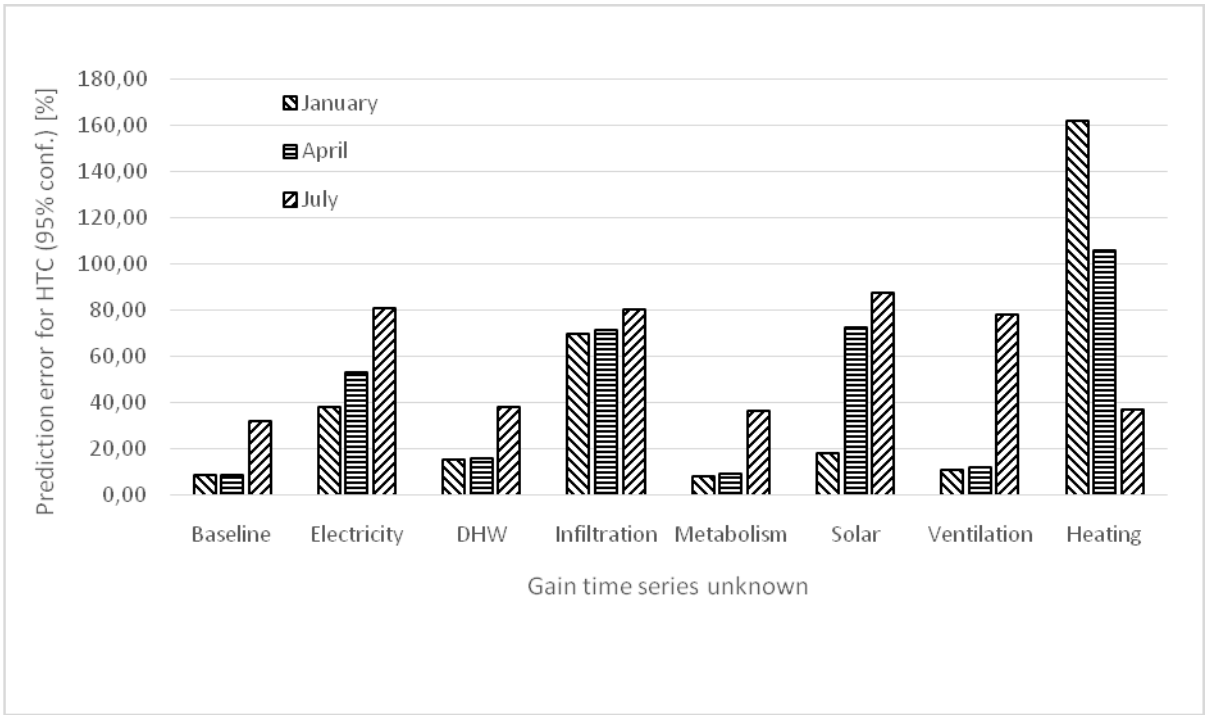

Figure 12 - Estimation errors of HTC over the 1000 buildings. The different bars represent January, April and July.

4.2.2. Internal temperature fitting

One of the applications of inverse modelling is the prediction of internal conditions in the building. For example, the model found for a building might be run using real weather in real time thereby allowing more accurate control of the building and its services, or predicted future weather under climate change might be used so likely future internal temperatures could be predicted.

The $AdjR^2$ for the eight scenarios and the three monthly periods is shown in Figure 13. The $AdjR^2$ shows that the LPM found is in most cases capable of providing a good fit, even in the scenarios in which one of the gains is missing. More than 97% of the estimations in winter in the baseline have an $AdjR^2$ larger than 60%, and more than 75% larger than 78%.

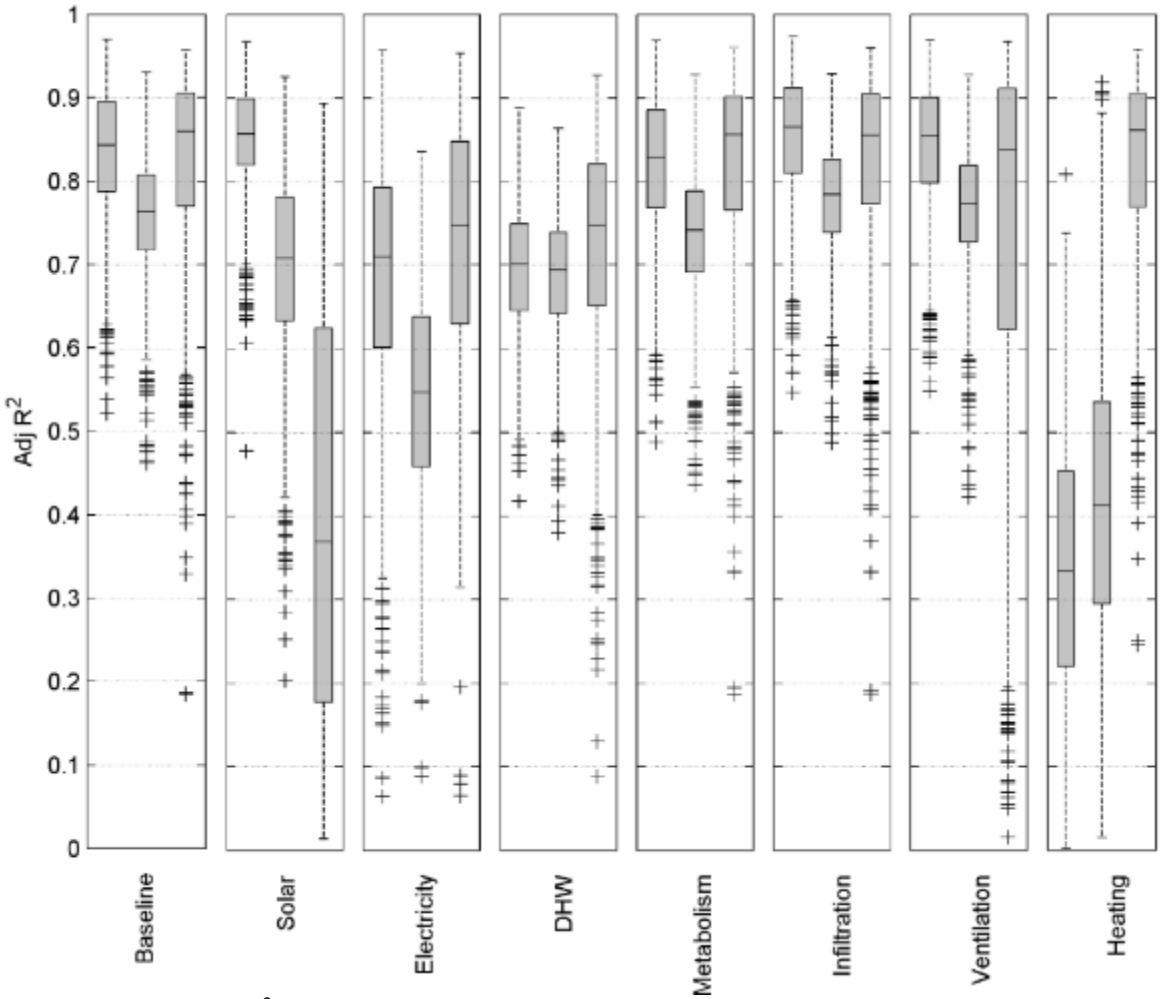

Figure 13 - Adjusted R^2 for the seven scenarios in January, April and July.

Only in the scenarios of *Solar* in July, *Electricity* in April and *Heating* in January and April are the majority of the AdjR^2 smaller than 60%. The fact that the temperatures are better represented in January and July is positive; it is in these months that phenomena such as heat waves and cold snaps are likely to happen. Being able to accurately predict the temperatures with IM has great potential for predicting the impact of such events on internal temperatures and hence occupants.

As an example, the fitting of House 2 in June is shown in Figure 14 for the scenario *Solar*, which applies inverse modelling without knowledge of solar gains. The fitting has an AdjR^2 of 0.307, and although the internal temperature of the LPM has similar mean as the internal temperature generated by EnergyPlus, it shows substantially different daily variations.

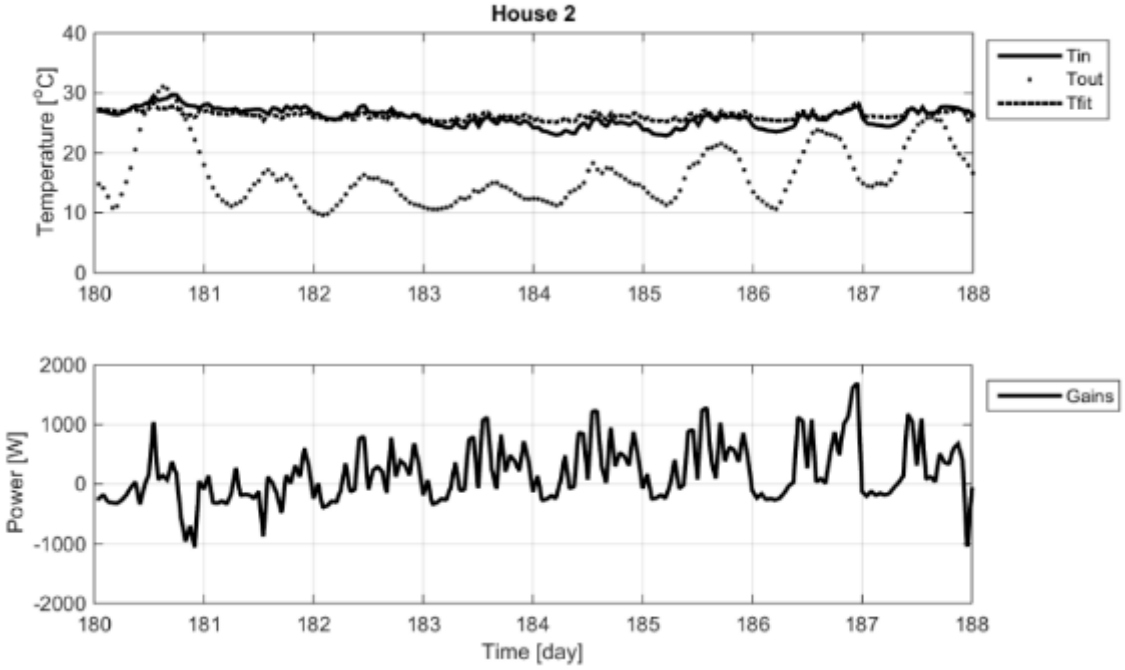

Figure 14 - Temperatures and gains for House 2 during 7 days of July (1-7th). In the upper subplot the dashed line is the internal temperature generated by the adjusted LPM, the solid line is the internal temperature generated by EnergyPlus, the dotted line is the external temperature. The total net gains are represented in the bottom subplot with the thick black line. This gains do not include solar gains as this is the *solar* scenario. The fitting has an $AdjR^2$ of 0.307.

4.3. Validation: Inverse modelling applied to specifically recorded data

In order to fully test the method, data was recorded in six real homes during the winter of 2015/16 (period chosen due to availability of data). Internal temperatures (in three locations per house), external temperature, electricity use, gas use (aggregated with DHW) and CO_2 concentration were obtained at a resolution of 5 minutes . Given the CO_2 concentration, it was possible to produce an estimation of the air renewal.

As in the models from EnergyPlus, we took the areas of each one of the elements of the building envelope from blueprints, and multiplied those by the U-Values of the constructions and windows obtained from . This gave us the HTC of the envelope of each one of the buildings. The constructions of the buildings, can be seen in Table 6.

Table 6 - Description of the set of homes in ENLITEN dataset.

	Floor area [m^2]	Type	Constructions, U-Values and description	
1	43.07	Terrace	Wall: 0.59 W/(Km^2) – Filled cavity (6c[2]) Windows: 2.7 W/(Km^2) – Double glazing Roof: 1.10 W/(Km^2)– Insulated roof (3b) Floor[3]: 1.39 W/(Km^2)– Insulated floor (1d)	
2	63.7	Flat	Wall: 1.44 W/(Km^2)– Cavity (6a) Windows: 2.7 W/(Km^2) – Double glazing Roof: n/a Floor: n/a	
3	37.8	Semi detached	Wall: 1.44 W/(Km^2) – Cavity (6a) Windows: 2.70 W/(Km^2) – Double glazing Roof:1.10 W/(Km^2)– Insulated roof (3b) Floor: 3.59 W/(Km^2) – Non-insulated floor (1d)	
4	53.72	Semi detached	Wall: 2.09 W/(Km^2) – Solid wall (3a) Windows: 2.7 W/(Km^2) – Double glazing Roof: 2.3 W/(Km^2) – Non-insulated roof (3a) Floor: 3.59 W/(Km^2)– Non-insulated floor (1d)	
5	54.72	Flat	Wall: 1.44 W/(Km^2) – Cavity (6a) Windows: 2.7 W/(Km^2) – Double glazing Roof: n/a Floor: n/a	
6	43.55	Semi detached (refurbished after photograph)	Wall: 0.59 W/(Km^2) – Filled cavity (6c) Windows: 2.70 W/(Km^2) – Double glazing Roof: 0.21 W/(Km^2) – Insulated roof (3f) Floor: 1.39 W/(Km^2) – Insulated floor (1d)	

The results for January are shown in Figure 15. In this graph, the estimated HTC is plotted against the known HTC.

[2] The codes in brackets are the construction identification code from CIBSE guide A. CIBSE (2006). Guide A: Environmental design. London, The Chartered Institution of Building Services Engineers .

[3] The U-Value of floor has been corrected with the ratio between monthly ground average ground temperature and air average temperature for the calculation of the HTC.

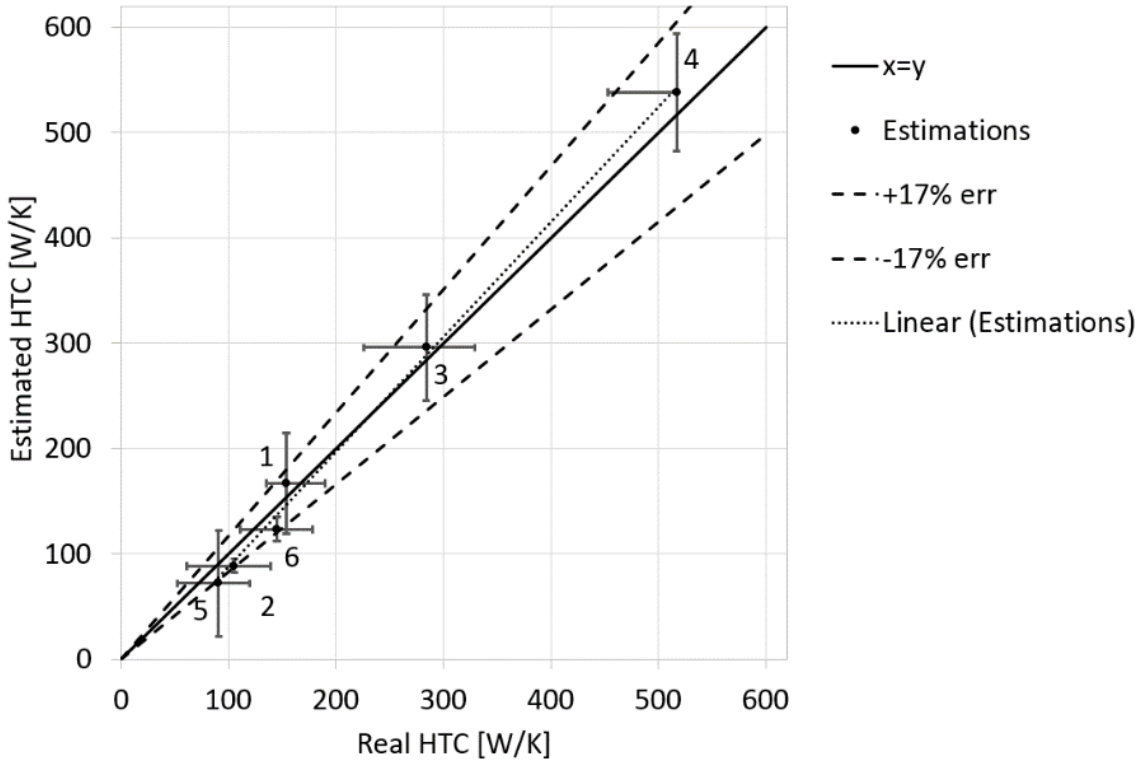

Figure 15 - Application of the inverse modelling engine to six real buildings, in Exeter, UK. The vertical error bars represent the deviations in the estimations using bedroom, living room and kitchen temperatures within each dwelling. The horizontal error bars represent the HTC that would result in selecting the next likely U-Value of the walls for each house.

The estimations in this exercise were corrected with the appropriate correction factors estimated in Section 4.2. In this case they compensate for the lack of knowledge of solar gains, DHW gains and metabolic gains.

It can be seen that the errors in the estimations are rather small. This is due to the ventilation rate being approximately known. In Figure 15, error margins of 17% are also shown, as these were the margins predicted in Section 4.2.1. The graph shows that this error prediction is accurate as well, as all points fall within these boundaries.

As the data available for this work was only for winter, the accuracy of the IM engine in obtaining the time constant was not evaluated as it was seen in section 4.1 that the method losses accuracy for estimating this parameter in this period.

5. Conclusions

This work is an attempt to see if the restricted data gathered from advanced smart meters or similar devices might be used to form the basis of a dynamic thermal model of a building. Given such a model, advice could be given that would, for example, provide the occupants with the savings that would arise from fitting insulation, or reducing the thermostat temperature, or turning the heating off one hour earlier. Unlike generic advice, based on typical U-values and typical occupants, this would be personalised and accurate to the building at hand and the way the occupants use the building. Such a model could also be used as a predictive controller, or to inform occupants or facility managers of any degradation in fabric or behaviour.

In a world in which the *internet-of-things* could make it commonplace to have inter-connected sensors even in a domestic environment, the application of these techniques is likely to show an explosive growth. However, to ensure that these techniques are applied correctly, more knowledge on how they work at the larger scale has to be gained. This paper is a first step towards this aim.

The work should be compared with previous work where inverse modelling was applied to a single building with several dozen sensors covering all gains and losses, including sensors capable of separating energy used for heating from that used for hot water, heat transfer in specific walls, cooking etc. and mapping window use and occupancy. In any real setting, it is unlikely that occupants would want such invasive monitoring, and the cost of the sensors and fitting them would be prohibit their use. It would be more likely that data will be sparse and irregular and its completeness case specific. Here, the accuracy of the approach was examined when much of this data is missing, as it would be in any practical use of the approach.

The methodology ensured that the thermal model topology used was applicable across 1000 common but diverse dwellings. These dwellings covered detached houses to apartments, of opaque U-Values of 0.1 to 2.16 W/(m^2K), infiltration of 0.04 to 1.2 ach, window-to-wall ratios of 7.5% to 33% and electricity annual demand of 10 to 81.5 kWh/(m^2year). At no point was the inverse modelling engine informed of the size, number of bedrooms or any other detail of the buildings.

It was found that there are certain gains that are needed to give useful results. Sensors recording heating, electricity and infiltration+ventilation are needed for estimations of the HTC in winter. If the internal conditions of the building are to be predicted in summer, some way of measuring solar gains will be required, but in general, the smaller difference between external and internal temperature makes it practically impossible to get accurate information about the thermal envelope of the building in summer.

This adds to the fact that the model works well when solar gains are small. The simple model deals poorly with radiative heat and therefore periods with high solar radiation may lead to poor estimations even when the solar gains are known. This should be taken into account when applying this methodology.

The approach was validated in a variety of real buildings. Data collected over winter at six buildings was used to confirm that the method correctly discovers the thermal properties of real buildings.

The validation phase reinforces the finding that an estimation of the air renewal is needed to have usable results. CO_2 levels have been seen to work well as a proxy for this.

Inverse modelling has been found to be a powerful tool that can provide real HTCs of a great variety of buildings and will outperform “clipboard-based” assessments or other methods, as it automatically treats each building as unique, and it is sensitive to the behaviour of the occupants.

6. Acknowledgments

The authors would like to thank EPSRC for funding this research under the project code EP/K002724/1.

7. Appendix I. Parameters considered in creating the SBS

In the following, the parameters used to describe each building are explained.

Building type: Considered a discrete random variable. The probability distribution was taken from the EHS . The probabilities can be seen inTable A1.

Table A1. Probabilities of each building type. From EHS (CLG 2007).

	dwellings in group (000s)	Percentage
Flat	4,792	20.60
Terrace	6,470	27.82
End-terrace and semi	5,804	24.95
Detached	6,187	26.60
Total	23,254	

Floor area and Infiltration:These parameters are correlated, with larger buildings having greater infiltration. This needs to be taken into account to ensure that the synthetic building stock reflects the true stock. To find this correlation measured infiltration and floor area data from the Micro CHP Acceleration project data set was used.

Floor area with infiltration showed a correlation with a p-value of 1.0132e-11, which is smaller than 0.05. Providing a two-variant normal random variable with mean[4] and covariance matrix:

Eq. A1

$$\mu = (4.53 \quad -0.978), \qquad C = \begin{bmatrix} 0.172 & 0.00958 \\ 0.00958 & 0.204 \end{bmatrix}$$

The histograms of floor area and infiltration and their correlation are shown in Figure A1.

Number of floors: The probability distribution of the number of floors was obtained from the EHS, giving Table A2.

[4] The mean values are [92.76 0.376] after applying the exponential function.

Table A2 - Percentage of dwellings with 1, 2 and 3 Storeys

Number of floors	**1**	**2**	**3**
Percentage [%]	8.974	87.18	3.846

Shared walls: In the case of a flat the number of shared walls can be any number between zero and three—due to a lack of data, the same probability of occurrence was assumed for these. In the case of a terrace, the number of shared walls is two and these are always opposite to each other. For semi-detached properties, the shared wall can be any of the four. Again, these have the same probability.

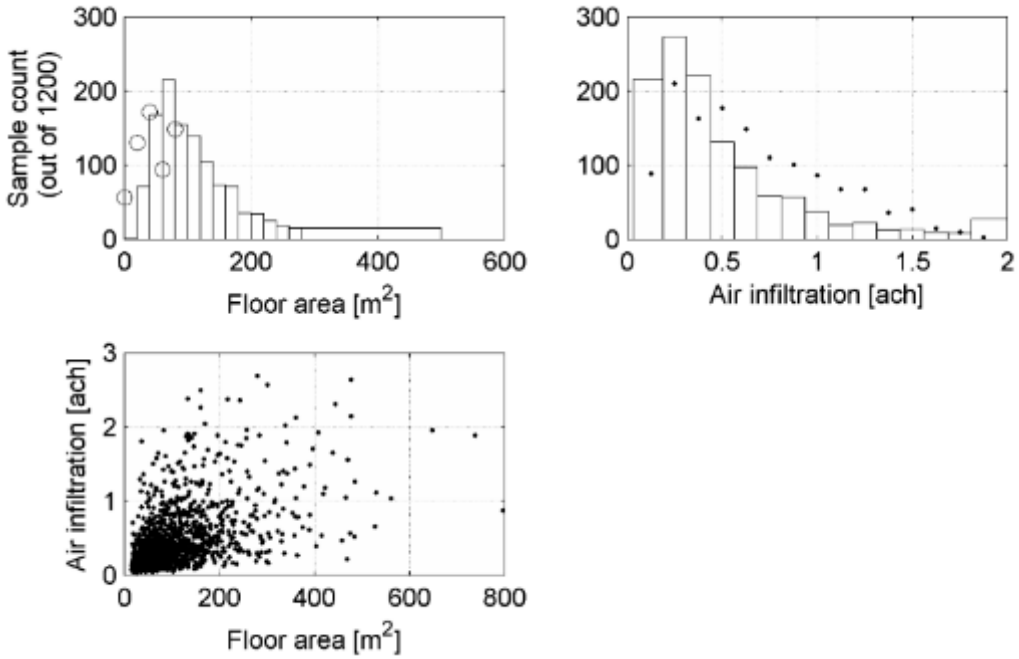

Figure A1 – Correlation between floor area and infiltration as a two-variant random variable. The circles in the top left graph represent the equivalent floor area histogram of the English Housing Survey and the dots on the top right graph represent the equivalent values of infiltration given in .

Aspect ratio: The aspect ratio was set as a random number ranging from 0.33 to 3 and following a uniform probability distribution.

U-Values: As in the case of floor area and infiltration, a correlation was seen between U-Values of walls and roofs. In this case the correlation had a p-value of 2.5729e-02, which is smaller than 0.05. Providing the following parameters[5]:

Eq. 2

$$\mu = (-0.453 \quad -1.269), \qquad C = \begin{bmatrix} 0.622 & 0.202 \\ 0.1026 & 0.237 \end{bmatrix}$$

The histograms of floor area and infiltration and their correlation are shown in Figure A2.

A filter was used to eliminate any sample in which the wall U-Value was out of the interval [0.1 – 3.02]. The upper bound representing a wall construction with the largest U-Value from and the lower bound a typical U-Value of a *Passivhaus* design.

For the roof, the maximum value allowed was 2.35 W/(m^{2}K), corresponding to Construction 2a Table 3.50 CIBSE Guide A (Flat Timber roof), and the minimum was also 0.1 W/(m^{2}K).

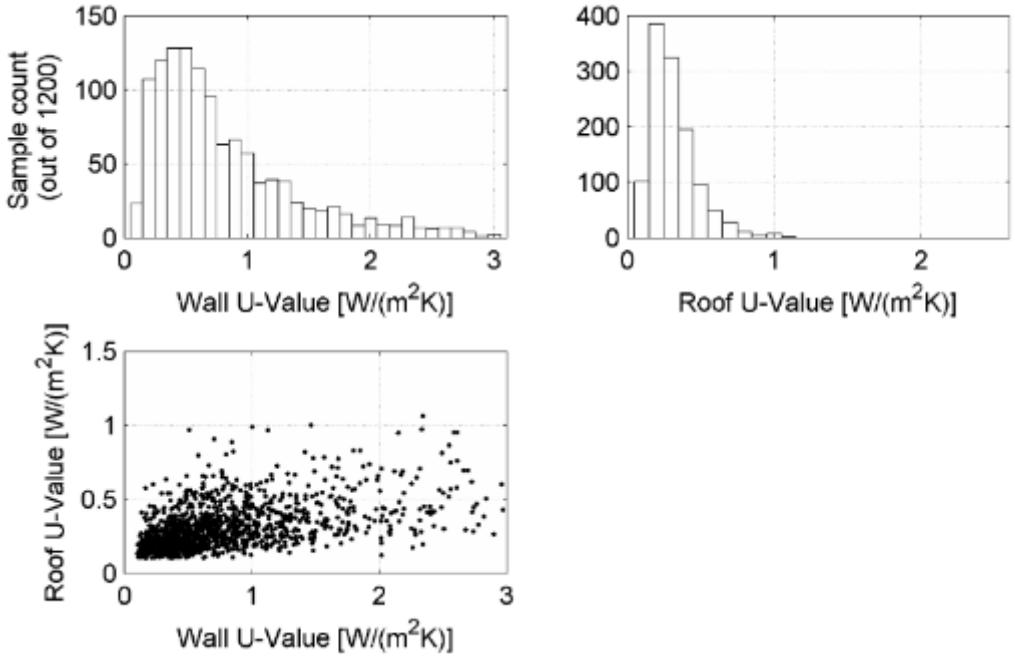

Figure A2 - Correlation of U-Values of walls and roof as a two-variant random variable.

[5] The mean values are [0.636 0.281] after applying the exponential function

Fenestration: This is sampled using a normal probability distribution with mean 19% and standard deviation 4.9%, these values were obtained from the CT database. The resultant probability distribution is similar to the one given by .

Window type: It was considered that windows can be single glazed, double glazed or triple glazed following the probability given by the EHS (shown in Table A3).

Table A3 - Probabilities of different window types

Type	**Probability**
Single	10.19%
Double	89.80%
Triple	0.01%

Thickness (thermal weight) of partitions: The partitions were assumed to be of concrete, with the thickness following a normal distribution with a mean of 50 mm and a standard deviation of 20 mm. All values smaller than 5mm were rejected. In terms of thermal mass, this covers cases from plasterboard to dense blocks.

Ventilation: Ventilation in dwellings is difficult to model and, in some cases, a “true” description of the habits of occupants does not even exist. Moreover, the human behaviour algorithms in the literature (such as the one in) do not cover residential window opening, and are not included in EnergyPlus.

Although modelling occupants’ habits with respect to window opening is rather complex, it is possible to determine the need of ventilation for air renewal and fresh air. On the one hand, the ventilation recommended to renew the air in a home is 3.5 l/(person s) according to ASHRAE ; on the other, ventilation to cool down the space should occur when the internal temperature gets out of the comfort region i.e. 28 degrees Celsius.

To implement these two regimes, a ventilation rate of 3.5 l/(person s) when occupied, and pro rata with the number of occupants was used. Also, the occupants are assumed to open the windows when the building has a temperature above 28 degree Celsius and it is occupied. As the ventilation rate suggested by ASHRAE may vary, ventilation has been left as a stochastic parameter (mean = 3.5 l/(s person) and σ = 1 l/(s person)).

Shading obstacles: It is assumed that each building is surrounded by four obstacles (to represent the landscape and other buildings) one in front of each of the facades of the building. The height of the obstacles is a random variable with a uniform probability distribution between zero and the height of the building. The distance from the obstacle to the facade has been fixed (4m), which results in the generation of a variable azimuth of the obstacle observed by the building. The ten first buildings generated with the building generator and their shading obstacles can be seen in Figure A3.

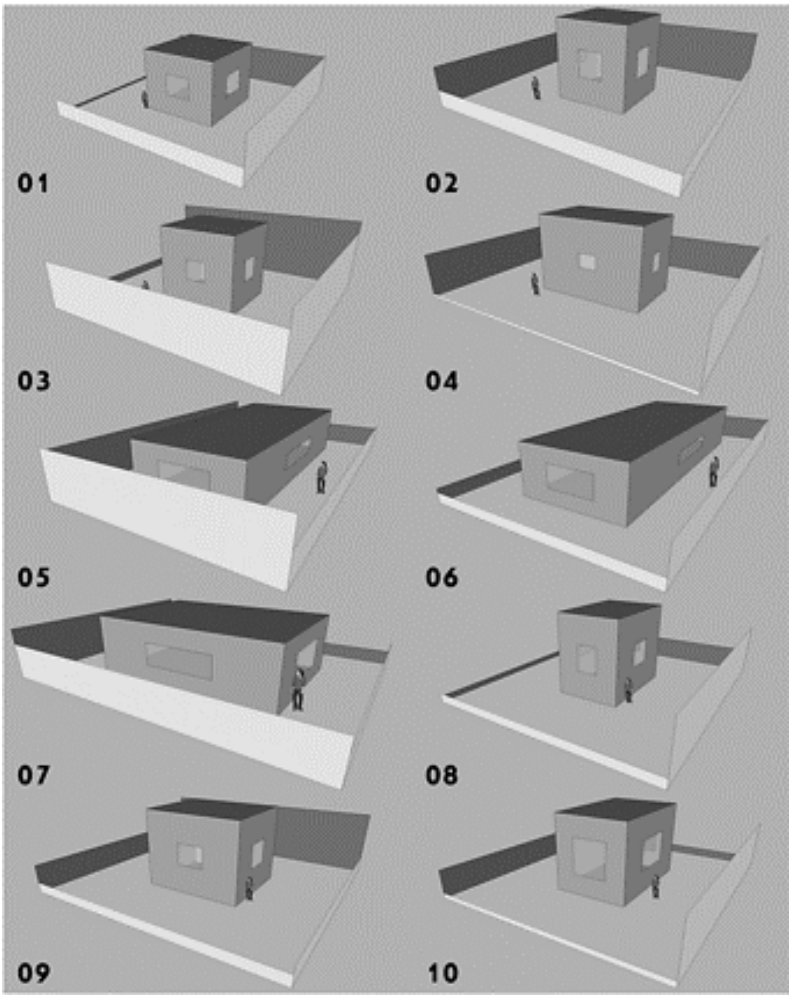

Figure A3 – Geometry of the ten first houses generated by the building simulator. These are the ones used in Section 3.4. Although the windows are shown as one per façade, one should imagine that these could be spread over the façade to get a more realistic picture; the one window approach is assumed as it reduces of simulation complexity, and because all buildings we modelled as single zone.

Electrical gains: For the electricity use, a hundred profiles were created with the tool of Richardson et al. . This profiles are generated in conjunction with those for occupancy to maintain temporal consistency. The average daily profile of the schedules used can be seen in Figure A4, the daily profile from the report of Owen and Foreman "*Powering the Nation*" is included for comparison. The report was used to obtain the mean and standard deviation of the annual electricity demand, giving a value of 38.10 kWh/(m^2year) for the mean and 17.95

kWh/(m^2year) for the standard deviation. Values smaller than 10 kWh/m^2 for year were excluded.

The resultant electricity time series can be seen in Figure A4.

Metabolic gains: The occupancy profiles are created in conjunction with the electricity profiles. The occupancy ratio can be seen in Figure A4. The activity level was set as 60W/person, in accordance to , when calculating the metabolic gains.

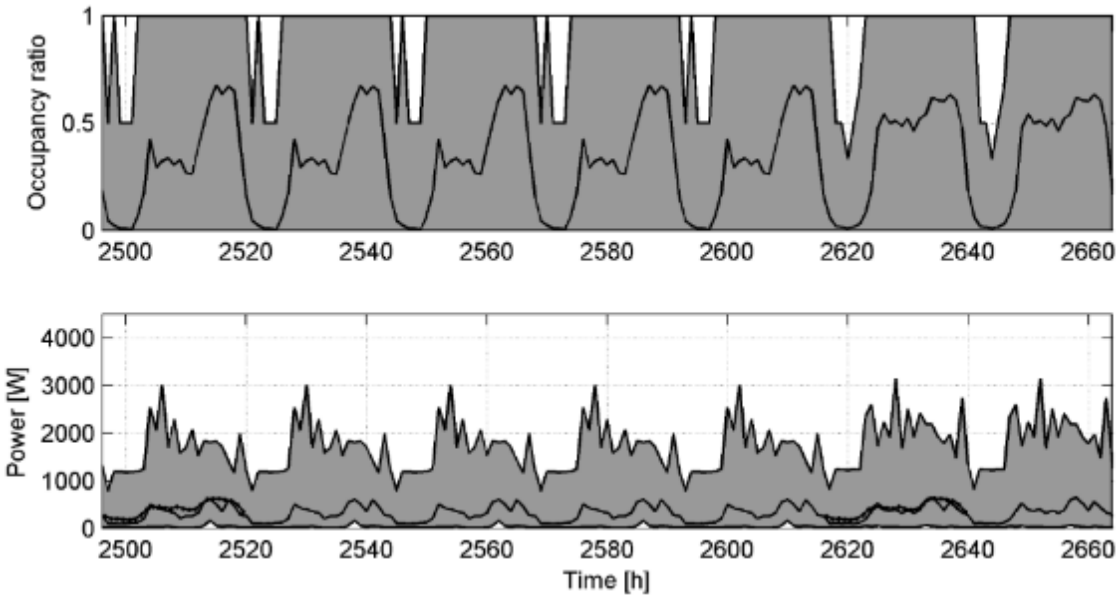

Figure A4 – Representation of the occupancy and electricity profiles. The grey area is the envelope of the profiles, the solid line the mean profile, and the dotted line in the lower subplot represents the daily profile given in the report of DECC: "*Powering the nation*".

Domestic hot water use: The report "Measurement of Domestic Hot Water Consumption in Dwellings" provides a mean and standard deviation for DHW of 1700 ± 220 kWh/(year dwelling).

The profile (time-series) for the DHW use was obtained with the NREL tool for DHW , and scaled accordingly to give the mean and deviation defined above. An example can be seen in Figure A5.

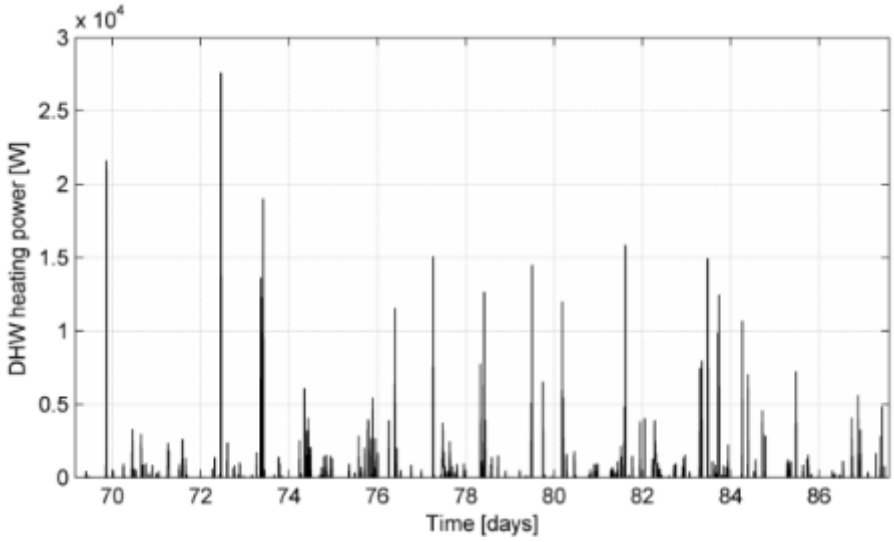

Figure A5 - Example of power profile used to produce Domestic Hot Water.

Most of the energy that is used to produce domestic hot water does not end up as gains in the thermal zone; instead, a large amount goes down the drain in the form of warm water. The only paper found in the literature concerning this issue was the one of Wong et al. that provides the energy exchanged with the environment in showers. No other information about other activities such as dish washing, bathing, or hand washing was found, therefore, the factor for heat exchange in showers was weighted with the proportion of hot water that is used in showers obtained from , and the result was an average value of 0.021 W/W (2.1% of the heat provided for hot water ends up heating the space). It should be noted that this ratio assumes that there are no pipe losses heating up the zone.

8. Appendix II

The following diagrams show the various lump-parameter building models that were tested.

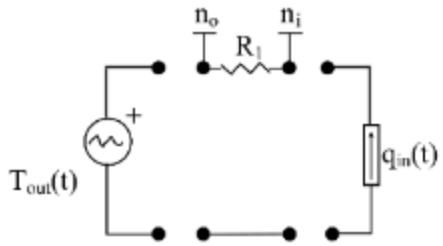

FigureAA1 - 1R model. This model has a single resistor that represents the thermal resistance of the building envelope. No inertial effects are considered with this model.

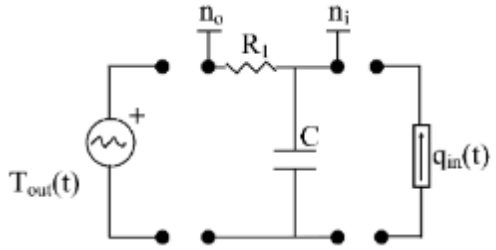

FigureAA2 - 1R1C model. First order model where the thermal resistance of the envelope is represented by R_1 and all the thermal mass of the building is represented by the capacitor C.

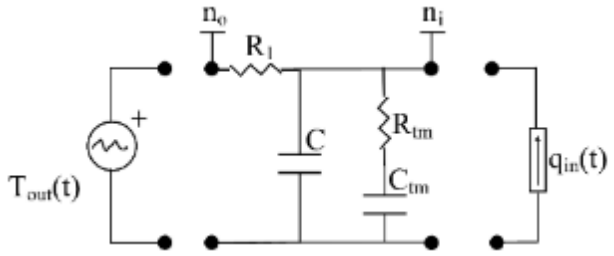

FigureAA3 - 1R1CTM model. This is the same as the 1R1C model, but the thermal inertia of the building is separated between the thermal inertia of the walls with the element C, and the thermal inertia of the thermal mass - which has its own time constant. This is represented with the resistor R_{TM} and C_{TM}.

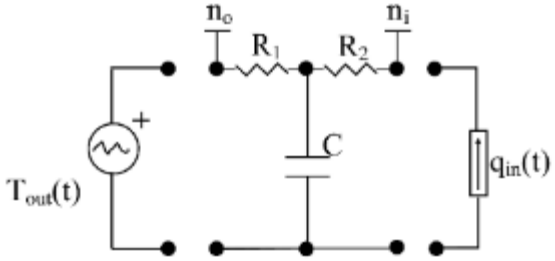

FigureAA4 - 2R1C model. This model is also first order like the 1R1C. However, the second resistor R_2 allows it to have different temperatures between the construction and the internal air, i.e. it has an extra degree of freedom. This allow to control the temperature swing due to gains $q_{in}(t)$.

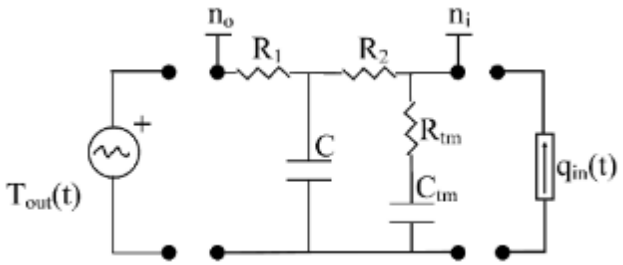

FigureAA5 - 2R1CTM model. This model is equivalent to the 2R1C model but it has the thermal mass included.

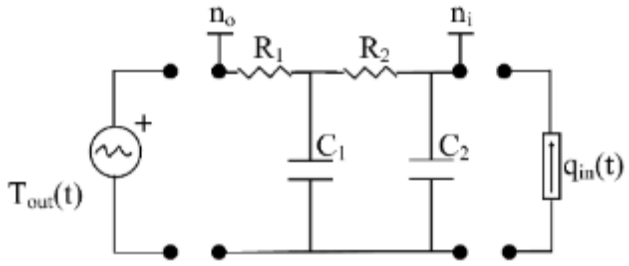

FigureAA6 - 2R2C model. This is a second order model with two time constants. R_1 C_1 provides the long-time constant of the building and relates with the thermal inertia of the constructions. The second time constant given by R_2 and C_2 is smaller and is used to represent quick response parts of the building such as the air within the spaces.

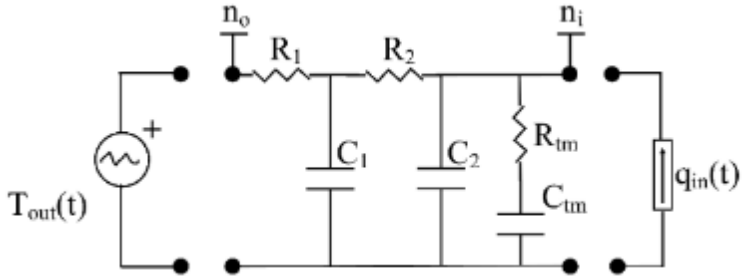

FigureAA7 - 2R2CTM model. As in previous cases, this is the 2R2C model with the thermal mass being represented.

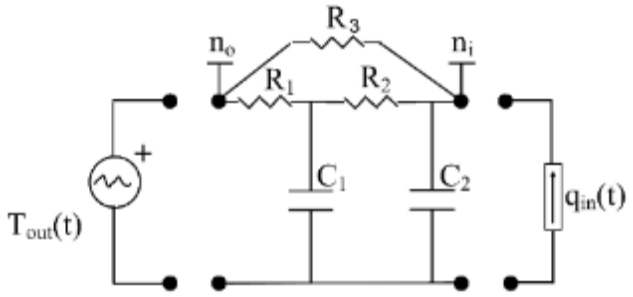

FigureAA8 - 3R2C model. This model adds the resistor R_3 to account for heat flows that bypass the thermal envelope of the building. This is considered to be the heat flow going through windows and infiltration and ventilation.

9. References

Andersen, K. K., H. Madsen and L. H. Hansen (2000). "Modelling the heat dynamics of a building using stochastic differential equations." Energy and Buildings **31**(1): 13-24.

ASHRAE (2009). *ASHRAE Handbook: Fundamentals*. Tullie Circle, N.E., American Society of Heating, Refrigerating & Air-Conditioning Engineers, Incorporated.

Bacher, P. and H. Madsen (2011). "Identifying suitable models for the heat dynamics of buildings." Energy and Buildings **43**(7): 1511-1522.

Boardman, B. (2007). Home truths: A low-carbon strategy to reduce UK housing emissions by 80% by 2050. U. o. Oxford. Oxford, University of Oxford's Environmental Change Institute.

BSi (2007). Thermal Performance of Building Components -Dynamic Thermal Characteristics- Calculation methods. London, BSI Group.

CIBSE (2006). Guide A: Environmental design. London, The Chartered Institution of Building Services Engineers

CLG (2007). English House Condition Survey, Annual report, Communities and Local Government.

Cole, W. J., K. M. Powell, E. T. Hale and T. F. Edgar (2014). "Reduced-order residential home modeling for model predictive control." Energy and Buildings **74**(0): 69-77.

Coley, D. A. and J. M. Penman (1992). "2nd-Order System-Identification in the Thermal Response of Real Buildings .2. Recursive Formulation for Online Building Energy Management and Control." Building and Environment **27**(3): 269-277.

Crawley, D. B., L. K. Lawrie, F. C. Winkelmann, W. F. Buhl, Y. J. Huang, C. O. Pedersen, R. K. Strand, R. J. Liesen, D. E. Fisher, M. J. Witte and J. Glazer (2001). "EnergyPlus: creating a new-generation building energy simulation program." Energy and Buildings **33**(4): 319-331.

CT (2008). Micro-CHP Accelerator. T. C. Trust. UK.

Date, J., A. K. Athienitis, Y. Chen and M. Fournier (2016). "Impact of thermal model resolution on peak heating demand calculation under different set point profiles." ASHRAE Transactions **122(1)**.

de Wilde, P. (2014). "The gap between predicted and measured energy performance of buildings: A framework for investigation." Automation in Construction **41**: 40-49.

DoE (2011) "London-Gatwick, weather datafile."

EST (2008). Measurement of Domestic Hot Water Consumption in Dwellings. DEFRA, Energy Saving Trust.

Fux, S. F., A. Ashouri, M. J. Benz and L. Guzzella (2014). "EKF based self-adaptive thermal model for a passive house." Energy and Buildings **68, Part C**: 811-817.

Ghiaus, C. (2006). "Equivalence between the load curve and the free-running temperature in energy estimating methods." Energy and Buildings **38**(5): 429-435.

Haldi, F. and D. Robinson (2011). "The impact of occupants' behaviour on building energy demand." Journal of Building Performance Simulation **4**(4): 323-338.

Hamilton, I. G., P. J. Steadman, H. Bruhns, A. J. Summerfield and R. Lowe (2013). "Energy efficiency in the British housing stock: Energy demand and the Homes Energy Efficiency Database." Energy Policy **60**: 462-480.

Hendron, R. and J. Burch (2007). Development of a standarised domestic hot water event schedules for residential buildings. N. R. E. Laboratory. U.S. Department of Energy, Office of Scientific and Technical Information, NREL.

IPCC (2014). Climate Change 2013: The Physical Science Basis, Intergovernmental Panel on Climate Change

Jiménez, M. J. and H. Madsen (2008). "Models for describing the thermal characteristics of building components." Building and Environment **43**(2): 152-162.

Kampf, J. H. and D. Robinson (2007). "A simplified thermal model to support analysis of urban resource flows." Energy and Buildings **39**(4): 445-453.

Kolokotsa, D., A. Pouliezos, G. Stavrakakis and C. Lazos (2009). "Predictive control techniques for energy and indoor environmental quality management in buildings." Building and Environment **44**(9): 1850-1863.

Lovett, T., E. Gabe-Thomas, S. Natarajan, E. O'Neill and J. Padget (2013). 'just enough' sensing to ENLITEN: a preliminary demonstration of sensing strategy for the 'energy literacy through an intelligent home energy advisor' (ENLITEN) project. Proceedings of the fourth international conference on Future energy systems. Berkeley, California, USA, ACM**:** 279-280.

Lundin, M., S. Andersson and R. Östin (2005). "Further validation of a method aimed to estimate building performance parameters." Energy and Buildings **37**(8): 867-871.

Mathews, E. H., P. G. Richards and C. Lombard (1994). "A First-Order Thermal-Model for Building Design." Energy and Buildings **21**(2): 133-145.

Nielsen, H. A. and H. Madsen (2006). "Modelling the heat consumption in district heating systems using a grey-box approach." Energy and Buildings **38**(1): 63-71.

Ogata, K. (2002). Modern Control Engineering. Upper Saddle River, New Jersey, Prentice Hall.

Owen, P. and R. Foreman (2012). Powering the nation. London, Energy Saving Trust.

Penman, J. M. (1990). "Second order system identification in the thermal response of a working school." Building and Environment **25**(2): 105-110.

Pérez-Lombard, L., J. Ortiz and C. Pout (2008). "A review on buildings energy consumption information." Energy and Buildings **40**(3): 394-398.

Rabl, A. and A. Rialhe (1992). "Energy signature models for commercial buildings: test with measured data and interpretation." Energy and Buildings **19**(2): 143-154.

Ramallo-González, A. P., M. Vellei, M. Brown and D. A. Coley (2015). "Remote facade surveying of windows characteristics." Energy Procedia **(In press)**.

Richardson, I., M. Thomson and D. Infield (2008). "A high-resolution domestic building occupancy model for energy demand simulations." Energy and Buildings **40**(8): 1560-1566.

Royer, S., S. Thil, T. Talbert and M. Polit (2014). "A procedure for modeling buildings and their thermal zones using co-simulation and system identification." Energy and Buildings **78**(0): 231-237.

Široký, J., F. Oldewurtel, J. Cigler and S. Prívara (2011). "Experimental analysis of model predictive control for an energy efficient building heating system." Applied Energy **88**(9): 3079-3087.

Tindale, A. (1993). "Third-order lumped-parameter simulation method." Building Services Engineering Research and Technology **14**(3): 87-97.

Wang, S. W. and X. H. Xu (2006). "Simplified building model for transient thermal performance estimation using GA-based parameter identification." International Journal of Thermal Sciences **45**(4): 419-432.

Wingfield, J., M. Bell, D. Miles-Shenton, T. South and B. Lowe (2011). Evaluating the impact of an enhanced energy performance standard on load-bearing masonry domestic construction, Understanding the gap between designed and real performance: Lessons from Stamford Brook. London, Department for Communities and Local Government.

Wong, L. T., K. W. Mui and Y. Guan (2010). "Shower water heat recovery in high-rise residential buildings of Hong Kong." Applied Energy **87**(2): 703-709.

Yang, J., H. Rivard and R. Zmeureanu (2005). "On-line building energy prediction using adaptive artificial neural networks." Energy and Buildings **37**(12): 1250-1259.